Investigation on global positioning system signal scattering and propagation over the rough sea surface*

Yang Chao(杨 超)†, Guo Li-Xin(郭立新), and Wu Zhen-Sen(吴振森)

School of Science, Xidian University, Xi'an 710071, *China*

(Received 21 July 2009; revised manuscript received 20 November 2009)

This paper is devoted to the study of polarization properties, scattering properties and propagation properties of global positioning system (GPS) scattering signal over the rough sea surface. To investigate the polarization and the scattering properties, the scattering field and the bistatic scattering coefficient of modified Kirchhoff approximation using the tapered incident wave is derived in detail. In modeling the propagation properties of the GPS scattering signal in the evaporation duct, the initial field of parabolic equation traditionally computed by the antenna pattern using fast Fourier transform (FFT) is replaced by the GPS scattering field. And the propagation properties of the GPS scattering signal in the evaporation duct with different evaporation duct heights and elevation angles of GPS are discussed by the improved discrete mixed Fourier transform taking into account the sea surface roughness.

Keywords: GPS signal, rough sea surface, electromagnetic scattering, propagation loss
PACC: 4110H, 9260V

1. Introduction

It is well known that the global positioning system (GPS) was first intended to be used for navigation and positioning. However, with the development of the GPS technology, GPS has been successfully used as a powerful remote sensing tool in the fields of geophysical information retrieval,[1−4] such as inversion of the sea surface roughness, the wind speed retrieval, the sea state monitoring, the ocean altimetry, etc. As we already know, atmospheric duct is ubiquitous in the oceanic environment,[5] when the GPS scattering signal passes through the atmospheric duct in the troposphere, the anomalous propagation of the GPS scattering signal may be caused by the special refractivity structure in the atmospheric duct, meanwhile, it is possible to acquire the refractivity information about the oceanic environment through the characteristics of GPS scattering signal propagation in the ducting environment. When the GPS signal impinges on the rough sea surface, two inextricably connected processes are mainly included, i.e. scattering and propagation. Traditionally, in modeling the radio wave propagation in the atmospheric duct, the initial field is often solved by the fast Fourier transform (FFT) according to the relation between the antenna pattern and the initial field distribution. But in the present study, which is unlike the previous work, our emphasis is placed on the propagation properties of the GPS scattering signal in evaporation duct, and the scattering field of the GPS signal is treated as the initial field to realize the process of propagation.

As far as the GPS signal scattering from the rough sea surface is concerned, among the rough sea surface scattering theories, the analytical model Kirchhoff approximation (KA)[6,7] and numerical model including the method of moment(MOM),[8] the finite difference time domain (FDTD)[9] method are the most common methods. In the present study, to overcome the artificial truncation and because the tapered incident wave[6] are closer to the actual radar wave than the plane wave, the polarization and the scattering properties of GPS signal from the rough sea surface are investigated with the modified KA by introducing the tapered incident wave which is commonly used in the MOM for calculating the rough sea surface scattering. Also the definition of the bistatic scattering coefficient in the modified KA is unified with that of the MOM, it is also found that the modified KA is more efficient than the MOM. In addition, the propagation proterties of the GPS scattering signal in the troposphere are studied by the most popular parabolic equation model solved by improved discrete mixed Fourier transform (IDMFT).[10,11] In what fol-

*Project supported by the National Natural Science Foundation of China (Grant No. 60971067), the Specialized Research Fund for the Doctoral Program of Higher Education, China (Grant No. 20070701010).
†Corresponding author. E-mail: yang_chaomail@163.com
© 2010 Chinese Physical Society and IOP Publishing Ltd

lows, the polarization properties, the scattering properties and the propagation properties of GPS signal in the oceanic environment are analysed in detail.

2. Scattering model from the rough sea surface

As shown in Fig. 1, considering an incident GPS signal $\varphi^{\rm inc}(\boldsymbol{r})$ impinging on a rough sea surface with the height profile $z = f(x)$.

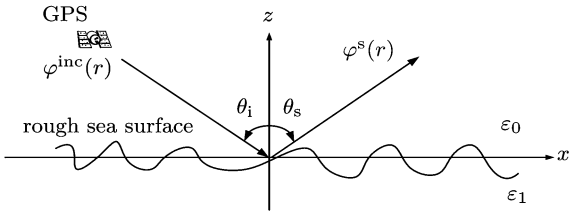


Fig. 1. Geometry of GPS signal scattering from the rough sea surface.

In the two-dimensional scattering problem $\boldsymbol{r} = x\hat{\boldsymbol{x}} + z\hat{\boldsymbol{z}}$, and the total field $\varphi(\boldsymbol{r})$ can be expressed as

$$\varphi(\boldsymbol{r}) = \varphi^{\rm inc}(\boldsymbol{r}) + \varphi^{\rm s}(\boldsymbol{r}), \tag{1}$$

where $\varphi^{\rm s}(\boldsymbol{r})$ is the scattered field, and can be written as[12]

$$\varphi^{\rm s}(\boldsymbol{r}) = \int_{\rm S} \left[\varphi(\boldsymbol{r}')\frac{\partial G(\boldsymbol{r},\boldsymbol{r}')}{\partial n'} - G(\boldsymbol{r},\boldsymbol{r}')\frac{\partial \varphi(\boldsymbol{r}')}{\partial n'}\right] {\rm d}s', \tag{2}$$

where $G(\boldsymbol{r},\boldsymbol{r}')$ is the two dimensional Green's function and $G(\boldsymbol{r},\boldsymbol{r}') = ({\rm i}/4)H_0^{(1)}(k_0\,|\boldsymbol{r}-\boldsymbol{r}'|)$, k_0 is the wave number, $H_0^{(1)}(\cdot)$ is the zeroth-order Hankel function of the first kind, and the normal derivative of the Green's function can be expressed as[13]

$$\frac{\partial G(\boldsymbol{r},\boldsymbol{r}')}{\partial n'} = \frac{{\rm i}\,k_0}{4}\hat{\boldsymbol{n}}'\cdot\frac{\boldsymbol{r}-\boldsymbol{r}'}{|\boldsymbol{r}-\boldsymbol{r}'|}H_1^{(1)}(k_0\,|\boldsymbol{r}-\boldsymbol{r}'|), \tag{3}$$

where $\hat{\boldsymbol{n}}' = [-f'(x')\hat{\boldsymbol{x}} + \hat{\boldsymbol{z}}]/\sqrt{1+[f'(x')]^2}$ is the unit normal vector of the rough sea surface and $f'(x')$ is the derivative of $f(x')$, $H_1^{(1)}(\cdot)$ is the first-order Hankel function of the first kind. Here, the Kirchhoff approximation is used to solve Eq.(2), then the total field on the surface is given by[12,14]

$$\varphi(\boldsymbol{r}') = [1+\Gamma]\varphi^{\rm inc}(\boldsymbol{r}'), \tag{4}$$

where Γ is the Fresnel reflection coefficient, and its expression will be presented in the next section. To avoid the error produced by the artificial truncation, the incident plane wave is replaced with the tapered plane wave introduced by Thorsos,[6] which contains a narrow angular distribution of energy with respect to the incident angle and can be described as

$$\begin{aligned}\varphi^{\rm inc}(\boldsymbol{r}') = {}& \exp\{{\rm i}\,k_0[x'\sin\theta_{\rm i} - f(x')\cos\theta_{\rm i}][1+w(\boldsymbol{r}')]\}\\ & \times\exp\{-[x'+f(x')\tan\theta_{\rm i}]^2/g^2\},\end{aligned} \tag{5}$$

where $w(\boldsymbol{r}') = [2(x'+f(x')\tan\theta_{\rm i})^2/g^2 - 1]/(k_0 g\cos\theta_{\rm i})^2$, $\theta_{\rm i}$ is the incident angle, and g is the tapering parameter. Typically, g is chosen to be a fraction of the length of the rough sea surface L. As the tapered incident wave is introduced, the tapering parameters g and L should at least satisfy all requirements of the wave equation, which results in[15]

$$g > \frac{6}{(\cos\theta_{\rm i})^{1.5}}, \tag{6}$$

$$L > 15l_c \cong 3.8U_{19.5}^2, \quad \text{and} \quad L \geq 4g, \tag{7}$$

where $l_{\rm c}$ is the correlation length of the sea surface, $U_{19.5}$ represents the wind speed in units of m/s, measured at a height of 19.5m above the sea surface.

The energy distribution of the tapered incident wave is presented in Fig. 2. Figure 2(a) indicates the energy distribution of the tapered incident wave in the upper space and Fig. 2(b) displays the amplitude distribution of the incident field on the rough sea surface. It is obviously that the field strength gradually attenuates from the centre to the edge of the rough sea surface, thus, it can effectively avoid the error produced by the artificial truncation.

From Eq. (1), the normal derivative of the total field can be written as[12,14]

$$\frac{\partial\varphi(\boldsymbol{r}')}{\partial n'} = (1-\Gamma)\frac{\partial\varphi^{\rm inc}(\boldsymbol{r}')}{\partial n'}, \tag{8}$$

where $\dfrac{\partial\varphi^{\rm inc}(\boldsymbol{r}')}{\partial n'} = (\nabla'\varphi^{\rm inc}(\boldsymbol{r}')\cdot\hat{\boldsymbol{n}}')$, and it can be rewritten as

$$\begin{aligned}\frac{\partial\varphi^{\rm inc}(\boldsymbol{r}')}{\partial n'} = {}& \varphi^{\rm inc}(\boldsymbol{r}')\Big[-f'(x')P_1 - f'(x')\\ & \times\frac{2(x'+f(x')\tan\theta_{\rm i})}{g^2}P_2 + P_3\\ & + \frac{2\tan\theta_{\rm i}(x'+f(x')\tan\theta_{\rm i})}{g^2}P_2\Big],\end{aligned} \tag{9a}$$

where

$$P_1 = {\rm i}\,k_0\sin\theta_{\rm i}(1+w(\boldsymbol{r}')), \tag{9b}$$

$$P_2 = \frac{2\,{\rm i}\,k_0[x'\sin\theta_{\rm i} - f(x')\cos\theta_{\rm i}]}{(k_0 g\cos\theta_{\rm i})^2} - 1, \tag{9c}$$

$$P_3 = -\,{\rm i}\,k_0\cos\theta_{\rm i}(1+w(\boldsymbol{r}')). \tag{9d}$$

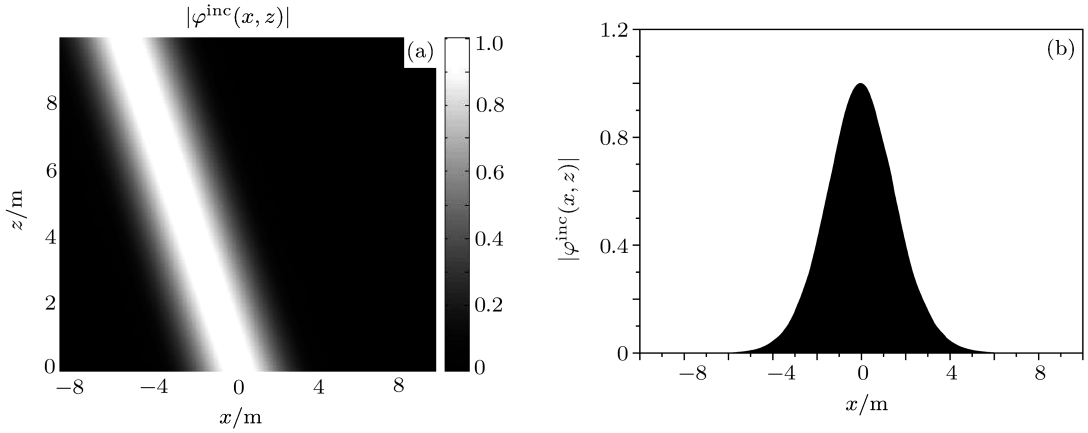


Fig. 2. Energy distribution of tapered incident wave.

Adopt the far field approximation, then the following relationship will hold for the argument of the Green's function, thus leading to $k_0\,|\boldsymbol{r}-\boldsymbol{r}'| \approx k_0 r - k_0\hat{\boldsymbol{r}}\cdot\boldsymbol{r}'$, where $\hat{\boldsymbol{r}}$ is the unit vector in the direction of $\boldsymbol{r}$. On the assumption that $k_0\,|\boldsymbol{r}-\boldsymbol{r}'| \gg 1$ or $k_0 r \gg 1$, the normal derivative of the Green's function can be calculated in a similar way. Consequently, the Green's function and its normal derivative can be rewritten as follows:

$$G(\boldsymbol{r},\boldsymbol{r}') \approx \sqrt{\frac{\mathrm{i}}{8\pi k_0 r}}\exp(\mathrm{i}\,k_0 r)\exp(-\mathrm{i}\,\boldsymbol{k}_{\rm s}\cdot\boldsymbol{r}'), \tag{10a}$$

$$\frac{\partial G(\boldsymbol{r},\boldsymbol{r}')}{\partial n'} \approx \sqrt{\frac{\mathrm{i}}{8\pi k_0 r}}\exp(\mathrm{i}\,k_0 r)\exp(-\mathrm{i}\,\boldsymbol{k}_{\rm s}\cdot\boldsymbol{r}')(-\mathrm{i}\,\boldsymbol{k}_{\rm s}\cdot\hat{\boldsymbol{n}}'), \tag{10b}$$

where $\boldsymbol{k}_{\rm s} = k_0(\sin\theta_{\rm s}\hat{\boldsymbol{x}} + \cos\theta_{\rm s}\hat{\boldsymbol{z}})$ is the scattering wave vector, and $\theta_{\rm s}$ is the scattering angle. Correspondingly, the scattering field under the Kirchhoff approximation can be presented as

$$\varphi^{\rm s}_{\rm KA}(r) = \sqrt{\frac{\mathrm{i}}{8\pi k_0 r}}\exp(\mathrm{i}\,k_0 r)\varphi^{(\rm N)}_{\rm KA}(\theta_{\rm s}), \tag{11a}$$

$$\varphi^{(\rm N)}_{\rm KA}(\theta_{\rm s}) = \int_{\rm S}\left[(1+\Gamma)\varphi^{\rm inc}(\boldsymbol{r}')(-\mathrm{i}\,\boldsymbol{k}_{\rm s}\cdot\hat{\boldsymbol{n}}') - (1-\Gamma)\frac{\partial\varphi^{\rm inc}(\boldsymbol{r}')}{\partial n'}\right]\times\exp(-\mathrm{i}\,\boldsymbol{k}_{\rm s}\cdot\boldsymbol{r}')\mathrm{d}s', \tag{11b}$$

$$\mathrm{d}s' = \sqrt{1+[f'(x')]^2}\mathrm{d}x'. \tag{11c}$$

The bistatic scattering coefficient $\sigma(\theta_{\rm s})$ is defined as[8]

$$\frac{P_{\rm s}}{P_{\rm inc}} = \int_{-\pi/2}^{\pi/2}\sigma(\theta_{\rm s})\mathrm{d}\theta_{\rm s}, \tag{12}$$

$P_{\rm inc}$ and $P_{\rm s}$ are the total power received by the rough surface and the scattered power by the rough surface, respectively. Finally, the bistatic scattering coefficients of the modified KA can be presented as

$$\sigma(\theta_{\rm s}) = \frac{|\varphi^{(\rm N)}_{\rm KA}(\theta_{\rm s})|^2}{8\pi k_0 g\sqrt{\dfrac{\pi}{2}}\cos\theta_{\rm i}\left[1-\dfrac{1+2\tan^2\theta_{\rm i}}{2k_0^2 g^2\cos^2\theta_{\rm i}}\right]}. \tag{13}$$

In our next numerical simulations, the one-dimensional rough sea surface profile with Pierson–Moskowitz (PM) spectrum is simulated by the Monte Carlo method.[16]

3. Propagation model over the rough sea surface

3.1. Boundary condition

Parabolic equation method have been developed and used extensively over the past twenty years to calculate the radio wave propagation problems due to its accuracy, stability, and importance that it can conveniently treat the influence of refractive index and the sea surface roughness on radio propagation in ducting environment. The impedance boundary condition[17] used in IDMFT can be expressed as

$$\left.\frac{\partial u(x,z)}{\partial z}\right|_{z=0} + \alpha u(x,z)|_{z=0} = 0, \tag{14}$$

where $u(x,z)$ is the field distribution, and α can be obtained from

$$\alpha = \mathrm{i}\, k_0 \sin\theta \left(\frac{1-\Gamma}{1+\Gamma}\right) \tag{15}$$

with α being the function of θ. Here, θ is the grazing angle at each range step of the rough sea surface, which is estimated by the spectral estimation method[18] in this work. The values of Fresnel reflection coefficient Γ for different polarization modes are given in the following. Subscripts H and V represent horizontal and vertical polarizations, respectively.

$$\Gamma_{\mathrm{H}} = \frac{\sin\theta - \sqrt{\varepsilon - \cos^2\theta}}{\sin\theta + \sqrt{\varepsilon - \cos^2\theta}},$$

and

$$\Gamma_{\mathrm{V}} = \frac{\varepsilon\sin\theta - \sqrt{\varepsilon - \cos^2\theta}}{\varepsilon\sin\theta + \sqrt{\varepsilon - \cos^2\theta}}, \tag{16}$$

where ε is the complex dielectric constant of sea water. In order to take the sea surface roughness into account, according to the rough surface theory and the Miller–Brown approximation, we introduce a modified Fresnel reflection coefficient[19]

$$\Gamma_{\mathrm{MB}} = \rho(\lambda,\theta)\Gamma, \tag{17}$$

where $\rho(\lambda,\theta)$ is the function known as the roughness reduction factor, which can be written as

$$\rho(\lambda,\theta) = \exp\left[-\frac{1}{2}(2k_0\zeta\sin\theta)^2\right] I_0\left[\frac{1}{2}(2k_0\zeta\sin\theta)^2\right], \tag{18}$$

where ζ is the root mean square (RMS) height of the rough sea surface, λ is the wavelength and I_0 is the modified Bessel function with the zeroth-order of the first kind. The RMS height of the rough sea surface is calculated through Phillips sea spectrum model[20]

$$\zeta = 0.0051 U_{19.5}^2. \tag{19}$$

Inserting Eqs. (18) and (19) into Eq. (17), we can obtain the modified Fresnel reflection coefficient. Hence, when the radio wave propagating over the rough sea surface is concerned, the Fresnel reflection coefficient Γ in Eq. (15) will be replaced by the modified Fresnel reflection coefficient Γ_{MB}.

3.2. Refractivity and modified refractivity

Generally, the refractive index n in the troposphere decreases with altitude increasing and the change of refractive index with altitude is negligibly small, however, this small change in refractive index causes the radio wave to be trapped in the atmospheric duct. Therefore, the concepts of refractivity N and modified refractivity M are used to express these small changes in refractive index, and N is defined as[21]

$$N = (n-1)\times 10^6. \tag{20}$$

The relation between M and N can be obtained from the following equation:

$$M = N + \left(\frac{z}{R_{\mathrm{e}}}\right)\times 10^6, \tag{21}$$

where z is the altitude and R_{e} is the Earth's radius. Differentiating Eq. (21) with respect to z yields

$$\frac{\mathrm{d}M}{\mathrm{d}z} = \frac{\mathrm{d}N}{\mathrm{d}z} + 157 \quad \mathrm{M\,units/km}. \tag{22}$$

Then in the presence of a tropospheric atmosphere duct, the inequality $\mathrm{d}N/\mathrm{d}z < -157$ units/km or equivalently $\mathrm{d}M/\mathrm{d}z < 0$ should be satisfied.

3.3. Improved discrete mixed Fourier transform

In terms of the impedance boundary condition, an auxiliary function w is introduced, i.e.

$$w = \frac{\partial u(x,z)}{\partial z} + \alpha u(x,z), \quad 0 \le z \le \infty. \tag{23}$$

Kuttler and Janaswamy[11] showed that the implementation of the discrete mixed Fourier transform (DMFT) with a central difference formula could lead to numerically unstable if $\Re e(\alpha)$ approaches zero. To solve this problem, Kutter replaced the central difference foumula with a backward difference formula in DMFT, and analysed its numerical stability and robustness theoretically. Consequently, the IDMFT is used to model the radio wave propagation over the sea surface in the following discussion. Firstly, in terms of the impedance boundary condition, backward difference formula is utilized to discretize an auxiliary function,[11] which results in

$$w(m\mathrm{d}z) = \frac{u(m\mathrm{d}z) - u[(m-1)\mathrm{d}z]}{\mathrm{d}z} + \alpha u(m\mathrm{d}z),$$
$$m = 1 : N-1 \tag{24}$$

with $w(0) = w(N\mathrm{d}z) = 0$, and $\mathrm{d}z$ being the height mesh space interval. According to Ref. [11], let $R = (1+\alpha\mathrm{d}z)^{-1}$, then multiply the Eq. (24) by $R\mathrm{d}z$, and define w' as

$$w'(m\mathrm{d}z) = R\mathrm{d}z\, w(m\mathrm{d}z) = u(m\mathrm{d}z) - Ru[(m-1)\mathrm{d}z],$$
$$m = 1 : N-1, \tag{25}$$

and then perform the discrete sine transform (DST) of $w'(m\mathrm{d}z)$, which yields

$$W'(j\mathrm{d}p) = \sum_{m=1}^{N-1} w'(m\mathrm{d}z) \sin\left(\frac{jm\pi}{N}\right), \quad j = 0 : N, \tag{26}$$

multiply $W'(j\mathrm{d}p)$ by the free space propagator $\mathrm{e}^{(\mathrm{i}\,\mathrm{d}x/2k_0)p^2}$, then we will obtain $W'(x+\mathrm{d}x, j\mathrm{d}p)$, and $w'(x+\mathrm{d}x, m\mathrm{d}z)$ that can be easily acquired from $W'(x+\mathrm{d}x, j\mathrm{d}p)$ by the inverse DST, i.e.

$$w'(m\mathrm{d}z) = \frac{2}{N} \sum_{j=1}^{N-1} W'(j\mathrm{d}p) \sin\left(\frac{jm\pi}{N}\right),$$
$$m = 0 : N, \tag{27}$$

where $\mathrm{d}x$ is the horizontal distance interval. Thus, $w'(x+\mathrm{d}x, m\mathrm{d}z)$ can be obtained and one can find the solution of Eq. (24). According to the theory of ordinary differential equations, the solution is just a combination of a particular solution u_p of the inhomogeneous equation and a linear combination of the general solutions to the homogeneous equation,[11] i.e.

$$u(m\mathrm{d}z) = u_\mathrm{p}(m\mathrm{d}z) + C_\mathrm{b} R^m, \tag{28}$$

where the particular solution u_p can be obtained from the following iterative formula by setting $u_\mathrm{p}(0) = 0$:

$$u_\mathrm{p}(m\mathrm{d}z) = w'(m\mathrm{d}z) + R u_\mathrm{p}[(m-1)\mathrm{d}z]. \tag{29}$$

The coefficient C_b[10] in Eq. (28) must be propagated to a new range step and can be calculated from the following equation:

$$C_\mathrm{b} = A(x) \exp\left[\frac{\mathrm{i}\,\mathrm{d}x}{2k_0}\left(\frac{\lg R}{\mathrm{d}z}\right)^2\right] - \sum_{m=0}^{N} u_\mathrm{p}(m\mathrm{d}z) R^m \tag{30}$$

with

$$A = \sum_{m=0}^{N} u(m\mathrm{d}z) R^m. \tag{31}$$

Finally, the field distribution can be obtained by multiplying $u(m\mathrm{d}z)$ with the environment propagator $\mathrm{e}^{(\mathrm{i}\,k_0/2)[n^2-1]\mathrm{d}x}$.

3.4. Initial field and propagation loss

It is well known that solving the parabolic equation is related to an initial value problem, and the field in range $x+\mathrm{d}x$ is dependent on the field at the previous range step, so one must begin with an initial field at range zero for propagating the field forward. In general, the far-field antenna pattern is used to calculate the initial field distribution by FFT. When we simulate the GPS scattering signal propagation in atmospheric duct, we assume that the GPS scattering field is regarded as the initial field in this paper, and the initial field is determined by Eq. (11a) with different scattering angles and observation distances for a fixed height mesh space interval. The geometry of the initial field is depicted in Fig. 3.

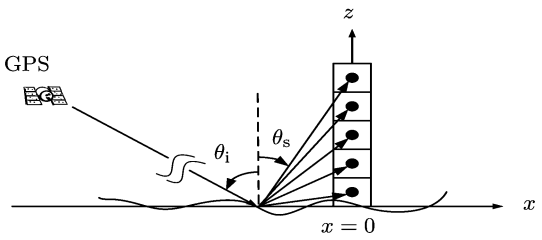


Fig. 3. Initial field of GPS scattering signal.

The research of the propagation loss on the radio wave propagation in the atmospheric duct is an important aspect in this area. Usually, the propagation loss[22] in dB is determined by the basic radio wave theory in the form of

$$L(x,z) = L_\mathrm{f} + 20\lg F, \tag{32}$$

where L_f and F denote the free space propagation loss and the propagation factor, respectively. Here, the free space propagation loss is given by the formula

$$L_\mathrm{f} = 32.45 + 20\lg f(\mathrm{MHz}) + 20\lg x(\mathrm{km}), \tag{33}$$

and the propagation factor F is defined as

$$F = \sqrt{x}\,|u(x,z)|\,, \tag{34}$$

where x is the propagation distance along x-axis, and z is the altitude measured with respect to the mean sea surface.

4. Numerical results and discussion

The GPS signal consists of two highly stable, almost monochromatic carriers, i.e. L1(1.57542 GHz) and L2 (1.2276 GHz), according to the concept of cut-off frequency[23] in atmospheric duct theory, the higher the frequency is, the more easily the atmospheric duct forms. As a result, the GPS signal L1(1.57542 GHz) is chosen in this work. In the following discussion, the field scattered by the rough sea surface can be calculated form Eq. (11a), the bistatic scattering coefficient and the propagation loss in the atmospheric duct are determined by Eqs. (13) and (32), respectively.

4.1. Polarization and scattering properties of GPS scattering signal

Usually, the elevation angle of GPS satellite coverage ranges from 5° to 60°, and the elevation angle of GPS satellite is defined as the complementary angle of the incident angle. To our knowledge, the GPS incident signal is right-handed circularly polarized wave. Suppose that the salinity and the temperature of the sea water are 20‰ and 20°, respectively, the dielectric constant of sea water is (72.45, 57.27), which is obtained from the empirical formula in Ref. [24]. To study the polarization properties of GPS signal scattered by the rough sea surface, the polarizability, the amplitude and the phase information of the GPS scattering signal are demonstrated subsequently. The polarizability is defined as the ratio of the vertically scattering field amplitude to that of the horizontally scattering field, and the observation distance is ten times the length of the wavelength. The randomly rough sea surface is created by 100 Monte Carlo realizations in the following numerical simulations.

Figure 4 shows the polarizabilities of the GPS scattering signal at different incident angles and wind speeds of 5 m/s and 10 m/s. From Fig. 4, it is readily seen that the polarizability decreases with the increase of incident angle for the same wind speed and large oscillations of the polarizability are obviously observed in Fig. 4(b) compared with those in Fig. 4(a), this phenomenon is attributed mainly to the fact that the larger the wind speed is, the rougher the sea surface will be.

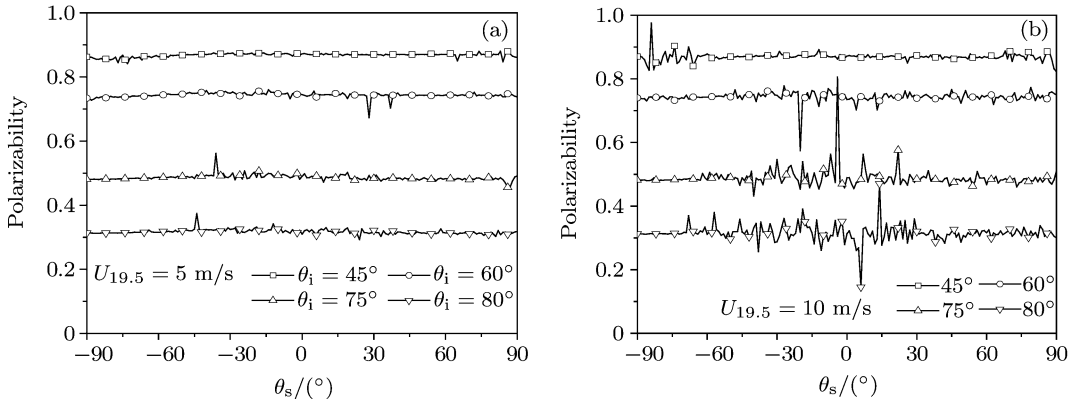


Fig. 4. Polarizabilities of the GPS scattering signal at different incident angles and wind speeds.

To further examine the polarization characteristics of the GPS scattering signal, the amplitude distribution and the phase difference of the GPS scattering signal are demonstrated in Fig. 5. Figure 5(a) illustrates the distribution of the vertically and horizontally polarized scattering fields, where the incident angle is $\theta_i = 75°$, the observation distance is ten times the length of the wavelength, and the wind speed is $U_{19.5} = 10$ m/s. Figure 5(b) displays the difference in phase between the vertically and horizontally polarized fields for the incident and the scattering fields. As illustrated in Fig. 5(a) the amplitude of the horizontally polarized scattering field is larger than that of the vertically polarized. In Fig. 5(b), because of the incident GPS signal is right-handed circularly polarized, the difference in phase of incident wave between vertically and horizontally polarized components is 90° and after scattering by the rough sea surface, the phase of the vertically polarized field related to the GPS scattering signal approximately falls by 73° behind the phase of horizontal polarized field, this result exhibits that GPS scattering signal is left-hand elliptical polarized, with the sea surface roughness considered.

Figures 6(a) and 6(b) describe the bistatic scattering coefficients of the GPS scattering signal for horizontal and left-hand elliptical polarizations at different incident angles, respectively. From Fig. 6, it is clearly found whatever the polarization is, the peak of the bisatic scattering coefficient appears around the specular direction, which is a logical result according to the Snell's law; besides it becomes larger with the incident angle increasing.

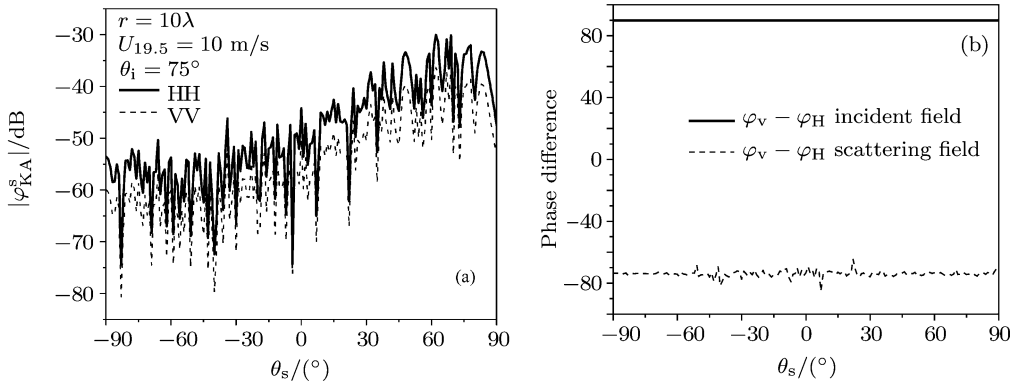


Fig. 5. Amplitude and phase difference of the GPS scattering signal.

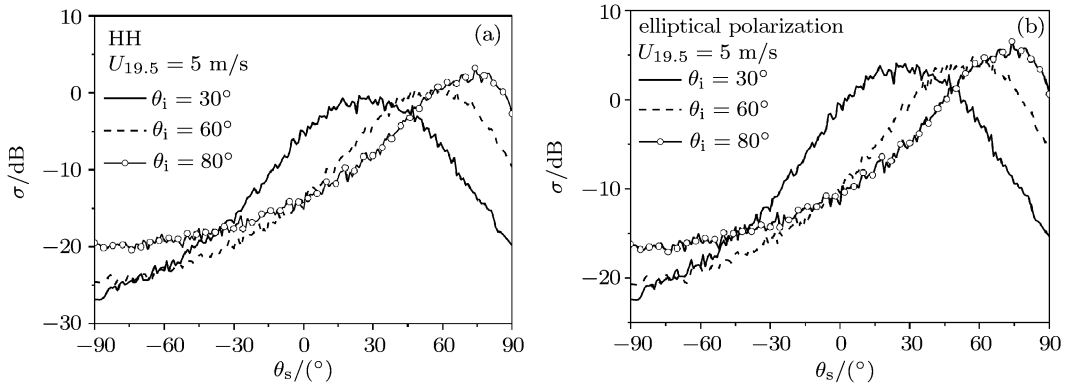


Fig. 6. Bistatic scattering coefficients of GPS scattering signal at different incident angles.

For exploring the influence of wind speed on the bistatic scattering coefficient of GPS scattering signal, the bistatic scattering coefficients at different wind speeds are plotted in Fig. 7. The bistatic scattering coefficients of GPS scattering signal for the horizontal and the elliptical polarizations at different wind speeds are presented in Fig. 7(a), it is obvious that the amplitude of the bistatic scattering coefficient of the elliptical polarization is larger than that of the horizontal polarization for the whole observation region under a fixed wind speed, which is mainly caused by the fact that the elliptically polarized wave is the superposition of the horizontally and the vertically polarized waves. Furthermore, the influence of the wind speed on the bistatic scattering coefficient is presented in Fig. 7(b). It is also seen that the amplitude of bistatic scattering coefficient for the elliptical polarization increases with the increase of the wind speed expect in the specular reflection direction, which is due to the fact that the lower the wind speed is, the smoother the sea surface will be, hence, the largest bistatic scattering coefficient is achieved around the specular reflection direction while the wind speed is 3 m/s.

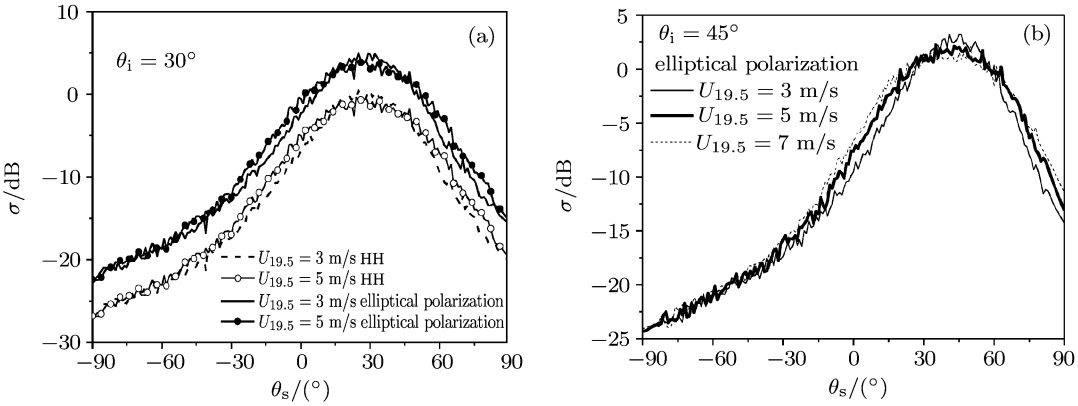


Fig. 7. Bistatic scattering coefficients of GPS scattering signal at different wind speeds.

4.2. Propagation properties of GPS scattering signal

The propagation properties of GPS scattering signal at different evaporation duct heights and elevation angles are presented in Figs. 8 and 9, respectively. Combining the numerical simulation of the field distribution from Eq. (28), the free space propagation loss from Eq. (33) and the propagation factor from Eq. (34), the propagation loss of GPS scattering signal is calculated from Eq. (32). Here, we take the evaporation duct for example to analyse the propagation properties, and the log refractive index profile[25] model is adopted, in which model modified refractivity $M(z)$ is specified, d is evaporation duct height, and $d = 0$ corresponds to the standard atmosphere, the refractive index n can be obtained from Eqs. (20) and (21). In Fig. 8, the receiver is located at an altitude of 10 m, the elevation angle of GPS is 5° and the wind speed is 10 m/s. It is found that all the curves of the propagation loss increase with the propagation distance increasing, on the whole, the higher the evaporation duct height is, the smaller the propagation loss for a fixed propagation distance will be.

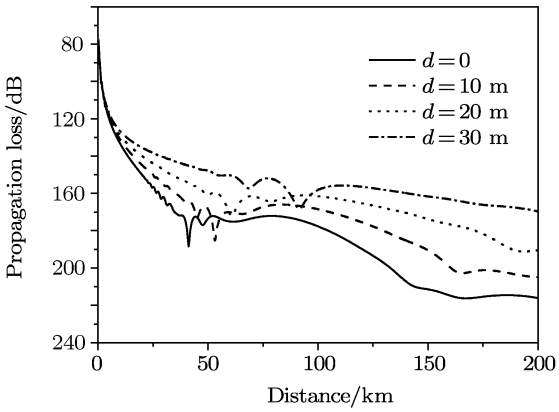


Fig. 8. Propagation losses of GPS scattering signal at different evaporation duct heights.

This phenomenon indicates that the trapping effect is enhanced with the raise of evaporation duct height. In Fig. 9, the evaporation duct height d is 30 m, i.e. $d = 30$ m and the other parameters are the same as those given in Fig. 8. It is clearly seen that the smaller the GPS elevation angle is, the less the propagation loss at a specified distance will be, in other words, the GPS scattering signal is more easily trapped in the evaporation duct at low elevation angles.

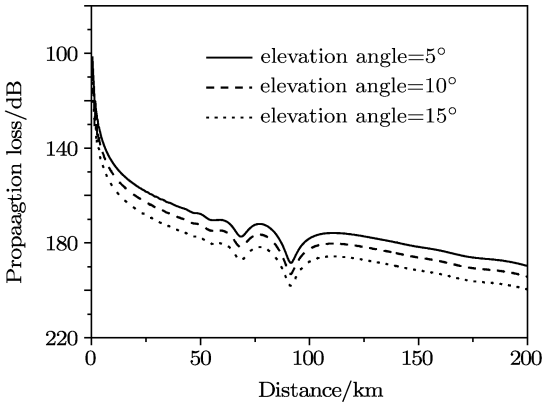


Fig. 9. Propagation losses of GPS scattering signal at different elevation angles.

5. Conclusions

The polarization properties, the scattering properties and the propagation properties of GPS scattering signal over the rough sea surface are presented. To study the polarization and the scattering properties of GPS scattering signal, the polzrizability, the amplitude, the phase, and the bistatic scattering coefficient of the GPS scattering signal are investigated, and the effects of the incident angle and the wind speed on the bistatic scattering coefficient are discussed. Moreover, the GPS scattering field is regarded as the initial field for analysing the propagation properties of GPS scattering signal in the evaporation duct at different evaporation duct heights and elevation angles of GPS satellite. The results obtained in this research can be expanded to the fields of engineering applications, such as communication, environmental remote sensing, design of GPS receiving antenna, etc. It should be noted that only the evaporation duct is concerned in this work, the surface duct will be considered in future work.

References

[1] Garrison J L, Komjathy A, Zavorotny V U and Katzberg S J 2002 *IEEE Trans. Geosci. Remote Sensing* **40** 5

[2] Lowe S T, Zuffada C, Yi Chao, Kroger P, Labrecque J L and Young L E 2002 *Geophys. Res. Lett.* **29** 1375

[3] Rius A, Aparicio J M, Cardellach E, Martin-Neira M and Chapron B 2002 *Geophys. Res. Lett.* **29** 2122

[4] Komjathy A, Armatys M, Masters D, Axelrad P, Za-

vorotny V and Katzberg S 2004 *J. Atmos. Oceanic Technol.* **21** 515
[5] Zhao X L, Huang J Y and Gong S H 2009 *Radio Sci.* **44** 106
[6] Thorsos E I 1988 *J. Acoust. Soc. Am.* **83** 78
[7] Wang R, Guo L X and Ma J 2009 *Chin. Phys.* B **18** 3422
[8] Tsang L, Kong J A and Ding K H 2001 *Scattering of Electromagnetic Waves: Numerical Simulations* (New York: John Wiely & Sons. Inc)
[9] Li J, Guo L X, Zeng H and Han X B 2009 *J. Opt. Soc. Am.* A **26** 1494
[10] Dockery G D and Kuttler J R 1996 *IEEE Trans. Ant. & Prop.* **44** 1592
[11] Kuttler J R and Janaswamy R 2002 *Radio Sci.* **37** 1021
[12] Ogilvy J A 1991 *Theory of Wave Scattering from Random Rough Surface* (Bristol: Institute of physics Publishing)
[13] Wang X D, Gan Y B and Li L W 2003 *IEEE Wireless and Propagation Let.* **2** 319
[14] Beckman P and Spizzichino A 1963 *The Scattering of Electromagnetic Waves from Rough Surface* (London: Pergamon)
[15] Ye H X and Jin Y Q 2005 *IEEE Trans. Ant. & Prop.* **53** 1234
[16] Li J, Guo L X and Zeng H 2008 *Waves in Random and Complex Media* **18** 641
[17] Kuttler J R and Dockery G D 1991 *Radio Sci.* **26** 381
[18] Guillet N, Fabbro V, Bourlier C and Combes P F 2003 *Geoscience and Remote Sensing Symposium* **7** 4186
[19] Freund D E, Woods N E, Hwar-Ching Ku and Awadallah R S 2006 *IEEE Trans. Ant. & Prop.* **54** 1292
[20] Levy M F 2000 *Parabolic Equation Methods for Electromagnetic Wave Propagation* (London: IEE Press)
[21] Sizun H 2004 *Radio Wave Propagation for Telecommunication Applications* (Berlin: Springer)
[22] Barclay L 2003 *Propagation of Radiowaves* (London: The Institution of Electrical Engineers)
[23] Liu C G and Pan Z W 1998 *Journal of China Institute of Communications* **19** 9
[24] Ellison W, Balana A, Delbos G, Lamkaouchi K, Eymard L, Guillou C and Prigent C 1998 *Radio Sci.* **33** 639
[25] Hitney H and Vieth R 1990 *IEEE Trans. Ant. & Prop.* **38** 794